

# Disentangling 3D from Large Vision-Language Models for Controlled Portrait Generation

Nick Yiwen Huang\*  
Brown University

Akin Caliskan  
Flawless AI

Berkay Kicanaoglu  
Flawless AI

James Tompkin  
Brown University

Hyeonwoo Kim  
Imperial College London

## Abstract

We consider the problem of disentangling 3D from large vision-language models, which we show on generative 3D portraits. This allows free-form text control of appearance attributes like age, hair style, and glasses, and 3D geometry control of face expression and camera pose. In this setting, we assume we use a pre-trained large vision-language model (LVLM; CLIP [36]) to generate from a smaller 2D dataset with no additional paired labels and with a pre-defined 3D morphable model (FLAME [26]). First, we disentangle using canonicalization to a 2D reference frame from a deformable neural 3D tri-plane representation. But, another form of entanglement arises from the significant noise in the LVLM’s embedding space that describes irrelevant features. This damages output quality and diversity, but we overcome this with a Jacobian regularization that can be computed efficiently with a stochastic approximator. Compared to existing methods, our approach produces portraits with added text and 3D control, where portraits remain consistent when either control is changed. Broadly, this approach lets creators control 3D generators on their own 2D face data without needing resources to label large data or train large models.

## 1. Introduction

Research into portrait generation now lets us create realistic 3D images via machine learning from photograph data-sets, with use in visual effects, games, and virtual reality. However, the problem of how to control the generation process to meet desired face attributes remains open. Such attributes may span hair color, face shape or expression, or age or hair style. Ideally, all of these attributes would be controllable independently so that, say, editing the hair style of a person does not change their expression.

Such controls are typically induced during learning

\*: The work was completed while Nick Huang was an intern at Flawless AI and back at Brown.

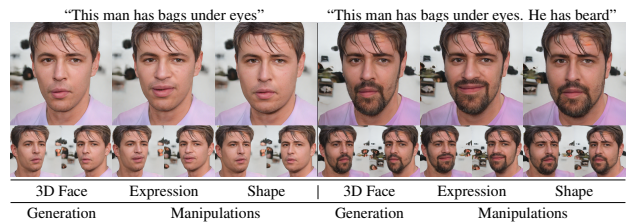


Figure 1. CLIPortrait allows text-guided 3D portrait generation and editing of 3D portraits. Given input text, CLIPortrait can synthesize high-quality 3D faces with disentangled geometry and camera control using parametric 3D face models.

through labels. Existing methods have focused on two label modes: 3D morphable models (3DMM) and text. 3DMMs are linear statistical models obtained from precisely-aligned 3D scan datasets [26, 34]. Fitting a 3DMM to a dataset allows conditioning a generator for precise control [2], but most 3DMMs are of the face or head only and so offer no appearance variation/control outside the 3DMM’s domain. Text is less precise but may allow easier high-level control, including all of the appearance. One approach is to pair matching photos and text labels of attributes, e.g., hair color, eye color, wearing glasses. However, every new attribute requires labeling, leading to a limited set of controls, limited sample size, or limited sample diversity. For instance, each photo in FFHQ-Text [59] has 9 text annotations, each describing a subset of 162 attributes for detailed geometry and appearance. But, the dataset only covers women, and has only 760 photos in total.

An alternative approach is to train a large vision-language model (LVLM) on many millions of in-the-wild photos and captions to define latent spaces that correlate text and images, e.g., the popular CLIP [36] model’s public release makes accessible a model that would be too costly to train for many. But, these models can be inconsistent: as each photo is not labeled with all desired text attributes, different geometry and appearance attributes end up *entangled* due to spurious correlations. Training a generator using CLIP

is a challenge: changing one attribute invariably changes another—an unsatisfying interaction.

To alleviate these limitations, we propose a method generate 3D portraits using both CLIP-derived text and 3D conditioning. This produces comparable quality and diversity of output to unconditional models but still allows independent control of geometry and appearance attributes across low, mid, and high levels. Our model is trained on a database of *unlabeled* 2D face photos (e.g., FFHQ [20]), using the pretrained LVLM CLIP and the 3DMM FLAME. Such an approach requires disentangling CLIP itself to isolate control over all parameters that could be controlled by FLAME, without damaging the ability of CLIP to describe diverse portraits—naïve approaches lead to low image quality, low sample diversity, or limited control. To disentangle, we learn to deform database faces to both 1) a 3D canonical space represented by a neural tri-plane, and to 2) a 2D canonical space in which CLIP can provide more reliable pseudo-labels that align text to images. In this way, CLIP only has to describe the appearance unexplained by the deformation and projection of a 3D volume into a camera. To bypass per-sample optimization, we define lightweight attribute mixing functions that can be baked from CLIP text prompts, e.g., ‘blue eyes’, ‘blonde hair’, for fast editing.

Beyond providing a model for high-quality controllable generation of 3D portraits, our approach more broadly defines a method to allow creators without the compute resources to train an LVLM directly to instead adapt one to their own smaller 2D face data, such as proprietary data from games or VFX studios, to allow text and fine-grained geometry control without expensive labeling.

It is worth noting that our contributions are orthogonal to specific LVLMs and 3D generative models. While we pick CLIP [36] as our LVLM and GNARF [2] as the generative backbone given their readily availability, our contributions are still applicable if, e.g., we swap CLIP with LLaVA [28] or replace GNARF with gaussian splatting models [7, 18, 22] or 3D diffusion models [23, 58] as long as they allow deformation for explicit geometry control.

## 2. Why LVLMs Struggle as 3D Labelers

Given a set of unlabeled images  $\hat{x} \in \mathcal{X}$ , we aim to construct a generator  $G(\mathbf{c}, \mathbf{z}) : \mathcal{C} \times \mathcal{Z} \rightarrow \mathcal{X}$  where  $\mathbf{c} \in \mathcal{C}$  denotes factors that allow us to control the generation process, and  $\mathbf{z} \in \mathcal{Z}$  denotes a noise vector accounting for the unexplained factors of variation in the synthesized appearance. To simply discussion, let  $\mathbf{c} = [\mathbf{c}_{\text{cam}}, \mathbf{c}_{\text{geo}}, \mathbf{c}_{\text{imp}}]$  where the camera pose  $\mathbf{c}_{\text{cam}}$  and the geometry  $\mathbf{c}_{\text{geo}}$  are explicitly controllable in a deformable 3D generative model. Anything we want to implicitly control by text, we leave in  $\mathbf{c}_{\text{imp}}$ . The goal is to induce  $\mathbf{c}_{\text{imp}}$  from free-form text prompts  $t \in \mathcal{T}$  to create photorealistic face images  $x$  that aligns with  $\mathbf{c}_{\text{imp}}$  while preventing  $\mathbf{c}_{\text{imp}}$  from a) interfering  $\mathbf{c}_{\text{cam}}$  and  $\mathbf{c}_{\text{geo}}$ . b) over-

shadowing  $\mathbf{z}$ . Our contributions focus on disentanglement; to explain this, first we consider why entanglement arises in LVLMs via their *alignment* objective.

**Alignment** Given text  $t$ , the alignment objective requires that the generated sample  $x$  be semantically consistent with  $t$ . Let  $E_{\text{txt}}(t) : \mathcal{T} \rightarrow \mathcal{R}$  be an encoder that maps text  $t$  to some representation  $\mathbf{r} \in \mathcal{R}$ ; likewise,  $E_{\text{img}}(x) : \mathcal{X} \rightarrow \mathcal{R}$  maps an image  $x$  to the same space  $\mathcal{R}$ . We can define the alignment of  $x$  to  $t$  as maximizing the mutual information  $I(x; t)$ , which is bounded by the mutual information  $I(\mathbf{r}_x; \mathbf{r}_t)$  between  $\mathbf{r}_x = E_{\text{img}}(x)$  and  $\mathbf{r}_t = E_{\text{txt}}(t)$ .

For CLIP,  $E_{\text{img}}$  and  $E_{\text{txt}}$  are trained with the InfoNCE objective. Oord et al. [33] show that minimizing InfoNCE maximizes the lower bound of  $I(\mathbf{r}_x; \mathbf{r}_t)$ , given text-image pairs  $(x, t) \in \mathcal{Y}$ :

$$\text{InfoNCE}(x, t) = -\mathbb{E}_{(x,t) \sim \mathcal{Y}} \left[ \log \frac{\exp(\cos(\mathbf{r}_x, \mathbf{r}_t))}{\sum_{x' \sim \mathcal{X}} \sum_{t' \sim \mathcal{T}} \exp(\cos(\mathbf{r}_{x'}, \mathbf{r}_{t'}))} \right] \quad (1)$$

$$\geq -I(\mathbf{r}_x; \mathbf{r}_t) + \text{constant} \quad (2)$$

CLIP was trained on Internet-scale 2D image/text data  $\mathcal{Y}$ . For a target dataset  $\mathcal{X}$  for which we would like a generator, say, the high-quality close-ups in FFHQ, let’s assume that CLIP happens to cover all portrait images. Then, text-guided 2D generation becomes viable even though FFHQ has no text labels: we can use  $\mathbf{c}_{\text{imp}} = \mathbf{r}_x = E_{\text{img}}(x_{\text{FFHQ}})$  to condition  $G$  during training, which requires no text labels. Then, at inference time, we replace  $\mathbf{r}_x$  by  $\mathbf{r}_t$ —this allows  $G$  to generate an image from any text prompt provided by the user. The contrastive objective while brings  $\mathbf{r}_x$  and  $\mathbf{r}_t$  as close as possible, does not fully eliminate the modality gap in  $\mathcal{R}$  [27] and instead causes entanglement in  $\mathbf{r}_x$  for our concerns.

**Entanglement.**  $\mathcal{Y}$  encompasses images of all things on the Internet—not just portraits with detailed text captions. This situation has two problems.

1) Only a small fraction of portraits in  $\mathcal{Y}$  contain a description of geometry, and the description is coarse, e.g., ‘smile’ does not define how wide the smile is, or ‘viewed from side on’ does not define the 3D camera angle. This allows  $E_{\text{img}}$  to encode incomplete geometry information  $\mathbf{r}_{x_{\text{geo}}}$  and camera information  $\mathbf{r}_{x_{\text{cam}}}$  in  $\mathbf{r}_x$  as the result of spurious correlations, e.g. celebrity faces are more likely to have a front camera pose and smiley expression. As such, introducing a 3D representation within the generator and then using  $\mathbf{r}_x$  as  $\mathbf{c}_{\text{imp}}$  leads to poor results since  $\mathbf{r}_{x_{\text{geo}}}$  and  $\mathbf{r}_{x_{\text{cam}}}$  are strongly at odds with  $\mathbf{c}_{\text{cam}}$  and  $\mathbf{c}_{\text{geo}}$ . For instance, if  $\mathbf{c}_{\text{cam}}$  specifies a camera pose different than what  $\mathbf{r}_{x_{\text{cam}}}$  dictates,  $G$  is ill-behaved as it receives conflicting conditions for the same control. We address this conflict by proposing 2D and 3D canonicalizations to eliminate  $\mathbf{r}_{x_{\text{cam}}}$  and  $\mathbf{r}_{x_{\text{geo}}}$  from  $\mathbf{r}_x$ . As long as all instances of  $x$  share the same camera pose and geometry, the generation process can no longer distinguish such information from  $\mathbf{r}_x$ .

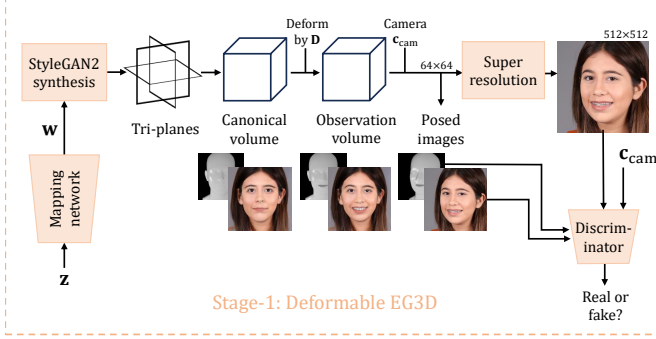


Figure 2. **Overview of Stage-1.** We use a deformable 3D generative model for Stage-1. We adapt GNARF [2] to improve the geometry conditioning of the discriminator using mesh renders.

2) The contrastive objective forces  $\mathbf{r}_x$  to be as discriminative as possible in  $\mathcal{Y}$ , but the most discriminative factors in  $\mathbf{r}_x$  could be irrelevant to portraits—non-portrait noise factors  $\mathbf{r}_{x_{\text{noise}}}$  can outweigh any useful factors when using  $\mathbf{r}_x$  as  $\mathbf{c}_{\text{imp}}$ . Examples of  $\mathbf{r}_{x_{\text{noise}}}$  include the camera used to produce the image, image format and quality, possible geographical location where the picture was taken (Fig. 6). We show in the supplemental that these noise factors can considerably overshadow factors that describe the person in the image. Since  $\mathbf{r}_{x_{\text{noise}}}$  is typically the most discriminative factors, it tends to be unique and vary greatly for different instances of  $x$ . As a result, this encourages  $G$  to be a deterministic function of  $\mathbf{r}_x$  and completely ignore  $z$ , since each  $x$  can be uniquely identified by just  $\mathbf{r}_{x_{\text{noise}}}$  (and therefore  $\mathbf{r}_x$ ). We avoid this degeneracy by introducing a Jacobian regularization that penalizes the generator’s sensitivity to  $\mathbf{r}_{x_{\text{noise}}}$ .

### 3. Method

#### 3.1. High-level Overview

Our overall approach is a 3D GAN (Fig. 3) that uses two training stages to disentangle CLIP for an unlabeled observation dataset  $\mathcal{X}$ . These two stages are necessary because our full model requires an unconditional deformable generator to obtain the canonicalized appearance condition  $\mathbf{r}_{\hat{x}}$ . Furthermore, bootstrapping our full model from an unconditional model helps avoid degenerate solutions caused by  $\mathbf{r}_{x_{\text{noise}}}$  which we show in Section 3.5.

**Stage-1 (Unconditional Generation)** First, we train a 3D generator  $G$  with no *a priori* text understanding to output a volumetric tri-plane representation (Fig. 2). This representation is deformed from its canonical format using a 3D map  $\mathbf{D}$  derived from 3DMM, and projected back to an intermediate low-resolution image  $x^\ddagger$  according to camera parameters  $\mathbf{c}_{\text{cam}}$  (Sec. 3.2). Finally, we use a super-resolution module to produce a sample  $x$  at desired target resolution from  $x^\ddagger$ . To train Stage-1, we use a discriminator to assess whether the rendered image  $x$  is real or fake and use an adversarial objective to optimize model  $G$ .

**Canonicalization** Once  $G$  is trained, we can canonicalize each sample  $x$  to a fixed-geometry 3D volume by inverting  $\mathbf{D}$ , and then render a frontal 2D image  $\hat{x}$  by inverting  $\mathbf{c}_{\text{cam}}$ . We run pre-trained CLIP on each canonicalized 2D image  $E_{\text{img}}(\hat{x})$  to compute  $\mathbf{r}_{\hat{x}}$ .

**Stage-2 (Conditioning Appearance on Text)** To add text control, we use an alignment network  $T_G$  to modify any random style vector  $w$  according to  $\mathbf{r}_{\hat{x}}$ . We disentangle 3D information from CLIP using 2D canonicalization such that  $\mathbf{r}_{\hat{x}}$  only contains frontal appearance information. The alignment network preserves the randomness of  $w$ , which maintains output diversity and enables interactive style mixing. Disentanglement of 3D information from CLIP occurs because  $\mathbf{r}_{\hat{x}}$  is predicted from 2D images that all share the same camera and geometry; any possible means to distinguish such information has been factored out of the generator.

#### 3.2. Generating Deformable 3D Portraits

We use a tri-plane reduction of a neural radiance field, like EG3D [5]. Given a 3D point, we query the tri-plane for a feature vector  $\mathbf{f}'$ , and obtain volumetric features  $\mathbf{f}$  and density  $\sigma$  from  $\mathbf{f}'$  using an MLP. We obtain a pixel of the low resolution render by integrating  $\mathbf{f}$  and  $\sigma$  along ray  $\vec{r}$ :

$$F(\vec{r}) = \int_{t_n}^{t_f} T(t)\sigma(t)\mathbf{f}(t)dt, \text{ where } T(t) = \exp\left(-\int_{t_n}^{t_f} \sigma(s)ds\right) \quad (3)$$

where  $t_n$  and  $t_f$  are the near and far bounds of the ray  $\vec{r}(t) = \mathbf{o} + \vec{\omega}t$  along the direction  $\vec{\omega}$  from the origin  $\mathbf{o}$ . Precise camera control is possible by changing the rays  $\vec{r}$  along which  $F$  is aggregated. To control portrait geometry, including face shape and facial expression, we deform the ray along which  $F$  is aggregated:

$$\mathbf{f}(\mathbf{x}') = \mathbf{f}(\mathbf{D}(\mathbf{x})), \quad (4)$$

where  $\mathbf{x}$  is a coordinate in the observation space and  $\mathbf{D} : \mathbb{R}^3 \rightarrow \mathbb{R}^3$  is a deformation that maps  $\mathbf{x}$  to a canonical space. Deforming coordinates from the canonical space removes the need for generator  $G$  to represent varying geometry.

$\mathbf{D}$  can be constructed from explicit 3DMMs. We use FLAME [26]: it has controllable parameters  $\beta \in \mathbb{R}^{100}$  for face shape,  $\theta \in \mathbb{R}^6$  for jaw and head pose, and  $\psi \in \mathbb{R}^{50}$  for facial expression. We estimate these for the observation mesh from  $\hat{x}$  using DECA [13]. We construct  $\mathbf{D}$  from FLAME analytically using the surface field (SF) method in GNARF by Bergman et al. [2]. SF derives the deformation field from the canonical mesh and the observation mesh aligned to  $\hat{x}$ . For the canonical space, we set the FLAME shape and expression coefficients to 0, but leave the jaw open to synthesize the mouth interior.

Given a target coordinate  $\mathbf{x}$ , SF locates its nearest triangle  $t_{\mathbf{x}}^D = [\mathbf{v}_0, \mathbf{v}_1, \mathbf{v}_2] \in \mathbb{R}^{3 \times 3}$  on the target mesh, and computes the barycentric coordinates  $[u, v, w]$  of the projection of  $\mathbf{x}$

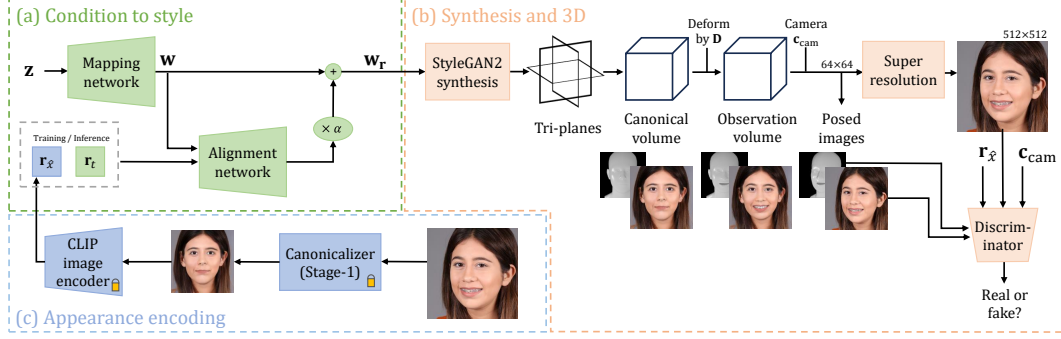


Figure 3. **Overview of Stage-2.** (a) The conditioning networks remap CLIP embeddings to a space  $w_r$  in which 3D information is ignored to be considered in stage (b), while noise vector  $z$  maintains sample diversity. (b) We synthesize a neural radiance volume via a tri-plane in a 3D canonical space, and with a particular appearance defined by  $w_r$ . Then, we deform this volume by FLAME parameters after fitting to the dataset. A discriminator judges the rendered output image. (c) The alignment network in (a) can only achieve a  $w_r$  free of 3D information if all generated images are ‘3D equivalent’; we achieve this via canonicalization.

on  $t_x^D$ . To calculate the deformed coordinate, we retrieve the corresponding triangle  $t_x^C$  on the canonical mesh and its normal  $\mathbf{n}_{t_x}^C$ :

$$\mathbf{D}(\mathbf{x}) = t_x^C \cdot [u, v, w]^\top + \langle \mathbf{x} - t_x^D \cdot [u, v, w]^\top, \mathbf{n}_{t_x}^D \rangle \mathbf{n}_{t_x}^C \quad (5)$$

which we use to query the canonical volume. Since geometry variations are explicitly controlled by deformation and have been factored out from  $G$ , entanglement between facial expression and camera pose in EG3D no longer exists; as such, we do not use generator pose conditioning [5].

Without informing the discriminator of the deformation, there is no guarantee that the deformed volume matches the expected deformation. To condition the discriminator, Bergman et al. [2] concatenate the camera pose with FLAME parameters. However, this leads to training instability, and sample quality is severely degraded even with the noise perturbation trick [2]. As Huang et al. showed [17], this is because the conditioning vector depends upon the unknown PCA basis for FLAME, making it difficult for the optimization to use this additional input. Instead, we adopt the Huang et al. method. We texture the mesh with its vertex coordinates in world space. Then, we render the observation mesh under  $\mathbf{c}_{\text{cam}}$  and concatenate the render  $rdr$  with  $x$  as input to the discriminator. We observe no training instability or quality degradation using this conditioning.

### 3.3. Canonicalization

Given our deformable EG3D, canonicalization can be reduced to an inversion problem. Specifically, the sample generation process of the deformable generator is given by:

$$w = M_G(z) \quad (6)$$

$$f = S_G(w) \quad (7)$$

$$x = V(f, \mathbf{c}_{\text{cam}}, \mathbf{c}_{\text{geo}}) \quad (8)$$

where  $M_G$  and  $S_G$  are the style mapping and synthesis networks of  $G$ ,  $V$  denotes deformable volume rendering.

For each image  $x$  in the training set, we estimate  $\mathbf{c}_{\text{cam}}$  and  $\mathbf{c}_{\text{geo}}$  using off-the-shelf models. The corresponding latent vector  $w_x$  can then be obtained by solving the following optimization problem:

$$w_x = \underset{w}{\operatorname{argmin}} \operatorname{DLPIPS}(V(S_G(w), \mathbf{c}_{\text{cam}}, \mathbf{c}_{\text{geo}}), x) \quad (9)$$

where  $\operatorname{DLPIPS}$  denotes the LPIPS distance that we use as our image similarity. Given  $w_x$ , we can now re-render the canonicalized  $\hat{x}$  under neutral camera pose and neutral geometry. We define the neutral camera pose  $\mathbf{c}_{\text{n.cam}}$  to be fully frontal and the neutral geometry  $\mathbf{c}_{\text{n.geo}}$  to have canonical FLAME parameters. The canonicalized  $\hat{x}$  is given by:

$$\hat{x} = V(S_G(w_x), \mathbf{c}_{\text{n.cam}}, \mathbf{c}_{\text{n.geo}}) \quad (10)$$

and the disentangled condition vector  $\mathbf{c}_{\text{imp}} = \mathbf{r}_{\hat{x}} = E_{\text{img}}(\hat{x})$ . Note that canonicalization happens before Stage-2 training as a data preprocessing step, and so it has no impact on the training time of Stage-2.

### 3.4. Conditioning on LVLM Text

We first visualize the importance of canonicalization in Figure 4: using the CLIP embedding from raw training images  $x$ , generation tries to incorrectly flatten faces to stay frontal regardless of the camera pose. Whereas conditioning on the canonicalized  $\mathbf{r}_{\hat{x}}$  produces correct geometry since neither  $G$  nor  $D$  can cheat with  $\mathbf{r}_{\hat{x}}$  for camera pose and geometry, and they must rely on  $\mathbf{c}_{\text{cam}}$  and  $\mathbf{c}_{\text{geo}}$  for such information.

To condition on  $\mathbf{r}_{\hat{x}}$ , it is possible to either train a new model from scratch that takes  $\mathbf{r}_{\hat{x}}$  as an input, or adapt our unconditional deformable model from Stage 1 to handling  $\mathbf{r}_{\hat{x}}$ . We choose the latter as we show in the following section that direct generation from  $\mathbf{r}_{\hat{x}}$  is prone to degenerate solutions due to the presence of  $\mathbf{r}_{\hat{x}, \text{noise}}$ . Our Stage 2 model splits conditional generation into two easier steps: unconditional generation (*i.e.* Stage 1) and alignment, where the latter seeks to modify an existing random sample such that

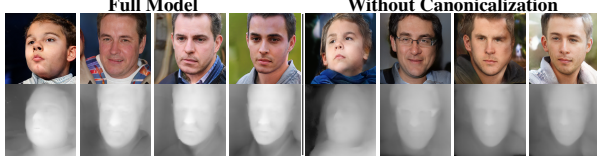


Figure 4. Without canonicalization before CLIP, faces look flat. Depth renderings of the estimated volume underneath show the more distorted space. [FFHQ 5mil. images.] This directly shows our major insight: the CLIP embedding of the uncanonicalized image inherently includes camera pose information that must be disentangled, else it confuses the 3D generation.

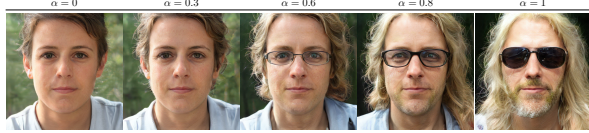


Figure 5. **Increasing  $\alpha$  increases prompt alignment.** *Text Prompt:* "Bearded man with long blond hair wearing glasses" CLIP correlates regular glasses and sunglasses as increasing "glasses" intensity, and we observe a similar phenomenon.

it aligns with  $\mathbf{r}_{\hat{x}}$ . Note that our Stage 1 model already facilitates well-behaved unconditional generation, as long as the alignment step is also well-behaved, we obtain well-behaved conditional generation on  $\mathbf{r}_{\hat{x}}$ .

Toward this goal, we introduce a CLIP alignment network  $T_G$  to  $G$  which predicts a personalized direction for the style vector  $w$  of a random sample, along which the sample gains alignment toward  $\mathbf{r}_{\hat{x}}$ :

$$w_{\mathbf{r}_{\hat{x}}}(\alpha) = w + \alpha T_G(w, \mathbf{r}_{\hat{x}}) \quad (11)$$

$\alpha \in [0, 1]$  is a scalar that controls the alignment strength, unless otherwise specified,  $w_{\mathbf{r}_{\hat{x}}}$  implies  $\alpha = 1$ . Similarly, we introduce an alignment network  $T_D$  to the discriminator  $D$  as follows:

$$u = S_D(x, r dr) \quad (12)$$

$$v = M_D(\mathbf{c}_{\text{cam}}) \quad (13)$$

$$v_{\mathbf{r}_{\hat{x}}}(\alpha) = v + \alpha T_D(v, \mathbf{r}_{\hat{x}}) \quad (14)$$

$$D(x | r dr, \mathbf{c}_{\text{cam}}, \mathbf{r}_{\hat{x}}) = u \cdot v_{\mathbf{r}_{\hat{x}}} \quad (15)$$

$S_D$  denotes the stem layers of  $D$  and  $M_D$  maps the camera pose to the condition vector for the EG3D discriminator. We implement  $T_G$  and  $T_D$  using a ResNet architecture and zero-initialize both networks to ensure that the extra condition  $\mathbf{r}_{\hat{x}}$  blends into our existing deformable EG3D smoothly.

### 3.5. Regularizing Noise in CLIP Embeddings

**Noise in CLIP.** We verify its existence by showing the similarity between face-related *main prompts* and *noise prompts* that are not related to the face description when both are compared against a CLIP image embedding of the target image. To show this, we generate text of FFHQ training images

using the third-party CLIP-Interrogator tool<sup>1</sup>. Given the generated text prompts, we split them into two groups: face-related (main prompt) and face-unrelated (noise prompt); Figure 6. Then, we evaluate *cosine* distance between CLIP image embedding and CLIP text embeddings.  $\mathbf{r}_{\hat{x}_{\text{noise}}}$  does exist and can outweigh the main facial appearance information in terms of cosine similarity. Furthermore, the average cosine similarity between the noise prompts and the entire FFHQ dataset shows that  $\mathbf{r}_{\hat{x}_{\text{noise}}}$  is unique enough to identify *each* corresponding training image.

**Distribution collapse from noise.** This leads to distribution collapse during training of the proposed network. After disentangling 3D control from  $\mathbf{r}_x$ , the remaining entanglement arises from  $\mathbf{r}_{\hat{x}_{\text{noise}}}$ . As  $\mathbf{r}_{\hat{x}_{\text{noise}}}$  is highly specific to each  $x$ , each  $x$  becomes identifiable solely from  $\mathbf{r}_{\hat{x}}$  and thus the conditional distribution  $p(x | \mathbf{r}_{\hat{x}})$  collapses to a delta distribution and all randomness of  $x$  is lost once  $\mathbf{r}_{\hat{x}}$  is determined.

Since  $G$  is trained to match  $p(x | \mathbf{r}_{\hat{x}})$ , it is encouraged to be a deterministic function of  $\mathbf{r}_{\hat{x}}$  and completely ignore the source of randomness  $\mathbf{z}$ , as sampling from  $p(x | \mathbf{r}_{\hat{x}})$  involves no randomness. This lack of randomness is highly undesirable for  $G$ : a generic prompt such as "a blond person" will be mapped to a single deterministic output rather than many diverse face images. This severely limits applications. Although we replace  $\mathbf{r}_{\hat{x}}$  with  $\mathbf{r}_t$  at inference time and  $\mathbf{r}_t$  contains no noise signal, the result will remain deterministic given that  $G$  has learned to dissociate  $\mathbf{z}$  during training.

For this dissociation to happen, either  $G$  has become a constant function w.r.t  $\mathbf{z}$ , or  $G$  is much more sensitive to the change of  $\mathbf{r}_{\hat{x}}$  than to the change of  $\mathbf{z}$ . More formally:

$$\frac{\partial G}{\partial \mathbf{z}} = 0 \quad (16)$$

$$\left\| \frac{\partial G}{\partial \mathbf{r}_{\hat{x}}} \right\|_{\text{F}} \gg \left\| \frac{\partial G}{\partial \mathbf{z}} \right\|_{\text{F}} \quad (17)$$

where  $\|\cdot\|_{\text{F}}$  denotes the Frobenius norm of the Jacobian.

To address Eq. (16), we force our model to retain the ability of unconditional generation by setting  $\alpha = 0$  with 50% probability during training. For unconditional generation,  $\mathbf{z}$  is the only input to the volume synthesis process. By forcing the distribution of unconditional generation to match the training distribution  $p(\mathcal{X})$ , it is encouraged to produce diverse samples, which is directly at odds with  $G$  being a constant function w.r.t  $\mathbf{z}$ .

For Eq. (17), a straightforward solution is to penalize  $\|\partial G / \partial \mathbf{r}_{\hat{x}}\|_{\text{F}}$ . However, this Jacobian term is too expensive to calculate. With the chain rule, we see that:

$$\left\| \frac{\partial G}{\partial \mathbf{r}_{\hat{x}}} \right\|_{\text{F}} = \left\| \frac{\partial G}{\partial w_{\mathbf{r}_{\hat{x}}}} \frac{\partial w_{\mathbf{r}_{\hat{x}}}}{\partial \mathbf{r}_{\hat{x}}} \right\|_{\text{F}} \leq \left\| \frac{\partial G}{\partial w_{\mathbf{r}_{\hat{x}}}} \right\|_2 \left\| \frac{\partial w_{\mathbf{r}_{\hat{x}}}}{\partial \mathbf{r}_{\hat{x}}} \right\|_{\text{F}} \quad (18)$$

<sup>1</sup><https://huggingface.co/spaces/pharmapsychotic/CLIP-Interrogator>




Input Image			
<b>Main prompt</b>	a close up of a person wearing a hat	a man with dreadlocks wearing a blue scarf	a close up of a person wearing a suit and tie
<b>Noise prompt</b>	ethnic group, canon eos 1000d, shot on anamorphic lenses, round dance, zun, emote, colored vibrantly	in 2015, resistance, quebec, black turtleneck, mineral, exploitable image	bondi beach in the background, loosely cropped, red carpet photography, post graduate, uncompressed png, anxious steward of a new castle, ultra high definition quality
<b>Cosine similarity with main prompt</b>	0.1838	0.2551	0.2273
<b>Cosine similarity with noise prompt</b>	0.3367	0.2701	0.3092
<b>Avg. cosine sim. with noise prompt across FFHQ</b>	0.1221	0.1248	0.1537

Figure 6. The comparison of cosine similarity between CLIP image embeddings of training images and CLIP text embeddings for prompts related to faces and those not related to faces. Noise prompts can have higher cosine similarity than face prompts. Further, the average cosine similarity between the noise prompts and the entire FFHQ dataset shows that  $\mathbf{r}_{\hat{x}^{\text{noise}}}$  is unique enough to identify *each* corresponding training image.

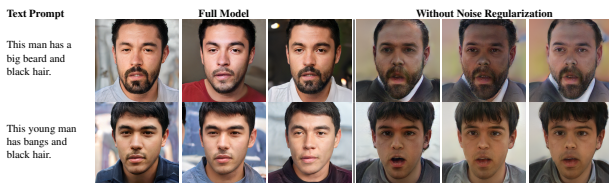


Figure 7. **Showing distribution collapse.** Our noise regularization improves diversity and quality. [FFHQ 5mil. images.]

$\partial G/\partial w_{\mathbf{r}_{\hat{x}}}$  is the computation bottleneck and not directly relevant to  $\mathbf{r}_{\hat{x}}$ , we thus omit this Jacobian term and penalize  $\|\partial w_{\mathbf{r}_{\hat{x}}}/\partial \mathbf{r}_{\hat{x}}\|_{\text{F}}$ , which penalizes the upper bound of  $\|\partial G/\partial \mathbf{r}_{\hat{x}}\|_{\text{F}}$ . We formulate this penalty as a regularization term  $R_{\mathbf{r}_{\hat{x}}}$  and apply a stochastic approximator for efficient compute:

$$R_{\mathbf{r}_{\hat{x}}} = \left\| \frac{\partial w_{\mathbf{r}_{\hat{x}}}}{\partial \mathbf{r}_{\hat{x}}} \right\|_{\text{F}}^2 \quad (19)$$

$$= \lim_{\sigma \rightarrow 0} \mathbb{E}_{\epsilon \sim \mathcal{N}(0, \sigma^2 I)} \left[ \frac{1}{\sigma^2} \|w_{\mathbf{r}_{\hat{x}} + \epsilon} - w_{\mathbf{r}_{\hat{x}}}\|^2 \right] \quad (20)$$

We show the proof of Eq. (20) in the appendix. Additionally, we notice that the norm of  $w_{\mathbf{r}_{\hat{x}}}$  has the tendency to grow uncontrollably, driving conditional generation results to unrealistic regions. We penalize norm growth:

$$R_{\text{norm}} = (\|w_{\mathbf{r}_{\hat{x}}}\| - \|w\|)^2 \quad (21)$$

when deriving conditional style vector  $w_{\mathbf{r}_{\hat{x}}}$  from unconditional  $w$  as in (11).

With our regularization techniques, we solve the distribution collapse problem allowing high-quality and diverse generation. Figure 7 verifies our hypothesis that the model cannot help but dissociate the source of randomness  $z$  under a stronger (text-)conditioning signal without the proposed Jacobian regularization. With both regularizers in place, we trade off a slight compromise in text-alignment overall

(‘bangs’). As a side control, we also provide a smooth transition from unconditional generation to conditional generation by manipulating  $\alpha$ , allowing the user to trade-off between alignment and fidelity (Fig. 9).

## 4. Experiments

**Datasets.** We use FFHQ [20] and Multi Modal CelebA-HQ (MMCelebA) [49] at  $512 \times 512$  resolution following prior work. While MMCelebA contains text annotations, we do not use any when training our model, and the data processing procedure follows exactly as in FFHQ.

We augment both datasets with horizontal flips and estimate the camera parameters for each image using an off-the-shelf model following EG3D. For FLAME parameter estimation, we adopt DECA to obtain initial results. The DECA estimates are not directly applicable due to the camera model differences between DECA (orthographic) and EG3D (perspective). We further optimize the initial estimates from DECA using a projected facial landmark loss to reconcile this difference. Finally, we optimize the scale and translation of the FLAME mesh to match the cropping of EG3D; other mesh postprocessing steps such as water-tightening and simplification follow GNARF.

**Model and Optimization.** For the EG3D backbone, we initialize the generator weights from the Egger et al. public checkpoint on FFHQ and largely follow their training routine and losses, including the non-saturating adversarial loss, R1 gradient penalty, and density regularization. However, we remove generator pose conditioning and lower learning rate  $\gamma = 0.001$  for both generator  $G$  and discriminator  $D$ . For faster deformation computation, we simplify the FLAME mesh to 2500 triangles, but use the full mesh for generating the mesh render  $rdr$  in discriminator conditioning. Lastly, we add our regularizations  $R_{c_x}$  and  $R_{\text{norm}}$  to the training objective, and empirically set their weights to 0.01 and 10.

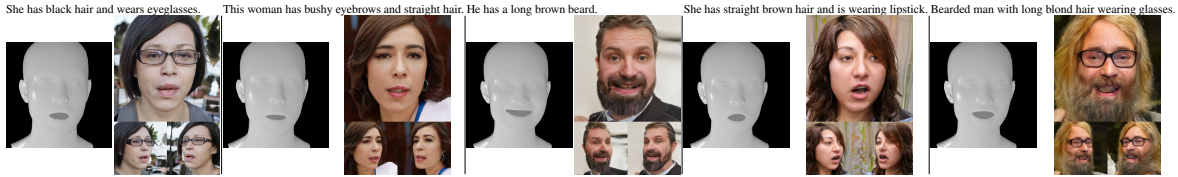


Figure 8. **Qualitative Evaluation** On text-to-3D portrait generation with explicit geometry control.

Method	FFHQ		Method	MM-Celeb-A-HQ	
	FID ↓	KID ↓		FID ↓	CLIP Score ↑
Text2Mesh* [30]	219.59	0.185	SEA-T2F [44]	93.8	20.8
ClipMatrix* [19]	198.34	0.180	ControlGAN [25]	74.5	21.3
FlameTex* [26]	88.95	0.053	AttnGAN [51]	51.6	21.5
CLIPFace* [1]	80.3	0.032	TG-3DFace [52]	39.0	22.7
CLIPPortrait	<b>5.87</b>	<b>0.00217</b>	CLIPPortrait	<b>31.8</b>	<b>23.1</b>

Table 1. Quantitative comparison. See Fig. 10 for a qualitative comparison. \*: These models are rasterization-based and cannot achieve the same level of fidelity as volume rendered models.

**Metrics.** For image generation quality, we use *Frechet Inception Distance (FID)* [15] and *Kernel Inception Distance (KID)* [3]. For semantic consistency, we use *CLIP score*, which is the *cosine* similarity between a CLIP image embedding and a CLIP text embedding.

#### 4.1. Comparison on Text-to-3D Face Generation

We evaluate the performance of CLIPPortrait on open-vocabulary text against the texture-mapping-based CLIPFace method [1] and generative TG-3DFace method [52]. In qualitative comparisons (Fig. 10, 8), we see improved image quality against CLIPFace and improved diversity and control against TG-3DFace. For quantitative evaluation, we compare with six additional text-guided 3D face generation methods (Tab. 1). On FFHQ [20], we evaluate the reality and diversity of rendered images by computing FID and KID scores using random samples for noise and CLIP embedding. On MMCelebA [49], we follow the same random sampling as FFHQ for FID score computation and we use provided text annotations for *CLIP score* computation. For experiment fairness, we use the given 3DMM coefficients associated with the samples. On both datasets, our method demonstrates higher fidelity and semantic consistency.

**Text-Image Matching Performance.** However, CLIP score is not a reliable measure on its own without FID. In Table 1, CLIPPortrait achieves good scores in both. But, in a comparison just of CLIP score, the CLIPFace method beats CLIPPortrait on the FFHQ-Text dataset [60] (Tab. 2). Since the authors do not provide the text prompts used in the original CLIPFace publication, we used the FFHQ-Text dataset to compute CLIP score. While it is higher, even distant inspection shows that samples created by CLIPFace do not look realistic. In contrast, our approach produces plausible appearance for the face as well as details in the hair or the presence of eyeglasses.

Method	CLIP Score	Generation Time	Text Prompts:			
			(a)	(b)	(c)	(d)
CLIPFace [1]	24.1	24 minutes				
CLIPPortrait	22.3	0.10 seconds				

Table 2. **CLIP score is a poor indicator of quality.** Our approach CLIPPortrait generates more plausible portraits than CLIPFace. Text prompts: (a) “She has blonde hair and wears eyeglasses” (b) “He has straight hair, and bags under eyes. He is wearing a necktie”, (c) “The person wears heavy makeup, necklace. She has arched eyebrows, and black hair”, (d) “This young person has brown hair”

Method	Text guidance	3D view consistency	3D geometry control	Appearance editing	Image only training	Photorealistic render
EG3D [5]	✓			✓	✓	
GNARF [2]	✓	✓		✓	✓	
Latent3D [4], Described3D [48]	✓	✓	✓			
TG-3DFace [52], DreamPortrait [6]	✓	✓	✓		✓	
CLIPFace [1]	✓	✓	✓	✓		
<b>CLIPPortrait (Ours)</b>	✓	✓	✓	✓	✓	✓

Table 3. Representative related methods in generative 3D face synthesis. Ours (CLIPPortrait) is the only method to allow text-guided synthesis of high quality 3D portraits with explicit geometry/camera control from an unlabelled 2D dataset.

**Inference Time Efficiency.** We present the generation speed of our method against CLIPFace in Table 2. The metrics were measured from the moment a new text prompt was inputted until the generation of a 3D portrait. Optimization-based text-to-3D face method CLIPFace [1] requires training from scratch for every new text prompt, resulting in a minimum time cost of 24 minutes. In comparison, CLIPPortrait achieves generation speed of approximately 0.10 seconds in the same settings with CLIPFace [1]. These results demonstrate the efficiency of our method in generating high-quality 3D-aware portraits from text prompts at smooth, nearly interactive frame rates.

## 5. Related Work

**3D-Aware Generative Face Synthesis.** GANs [8, 20, 21] became increasingly popular in the last decade for creating

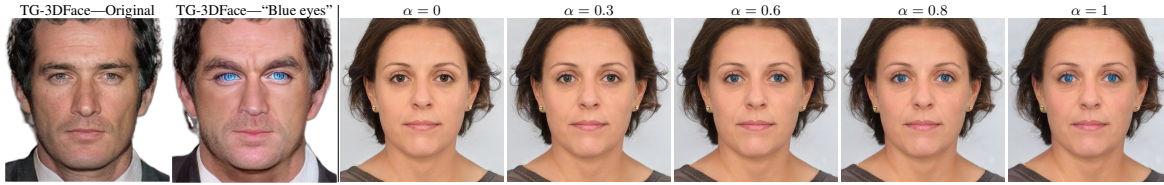


Figure 9. Text-guided 3D face appearance manipulation. Increasing  $\alpha$  increases prompt alignment, which is not possible in TG-3DFace [52]. As there is no public TG-3DFace [52] code, we took images from their original paper and used the same “blue eyes” prompt.

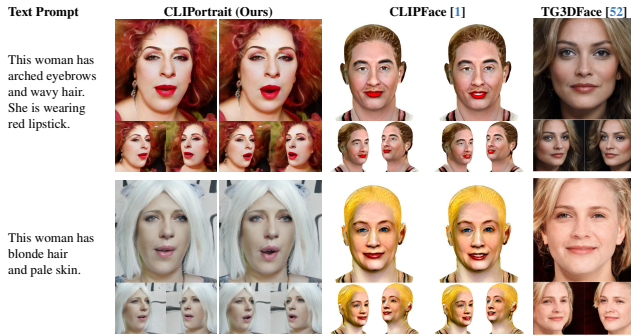


Figure 10. **Text and 3D control (face shape, expression, and camera).** Our method shows improved quality against CLIPFace [1], and improved diversity and control against TG3DFace [52], which cannot vary face shape or expression. These examples have  $\alpha = 1$ , showing the most strong or dramatic response to the text prompt, e.g., very red lips or very blonde (white) hair.

high-quality photo-realistic images. Recent works have used 3D-aware multi-view consistent GANs from a collection of single-view 2D images in an unsupervised manner. The key idea is to combine differentiable rendering with 3D scene representations such as meshes, point clouds, voxels, and implicit neural representations. Among these representations, neural implicit representations [5] have recently become a major focus of attention due to their superior rendering quality. Even though previous 3D-aware GANs can control camera viewpoints, they lack precise and semantically coherent control over the geometry and appearance attributes. To tackle geometry control, recent works [2, 50] propose articulated generative 3D faces with 3D parametric model control. For appearance control, [52] achieves text-guided 3D face generation without precise geometry control. In contrast, our method offers control over both appearance and geometry in the generation of 3D faces.

**Text-to-3D Face Generation.** The goal here is to produce an image that visually depicts a text description. This can be accomplished with GANs [11, 25, 39, 45, 51, 54, 55, 61], auto-regressive models [9, 10, 12, 24, 37, 37, 46, 53, 57] and diffusion models [16, 32, 38, 41, 42]. Some works focus on text-guided facial image generation [31, 35, 43, 44, 47, 49]. However, these methods only generate single-view images

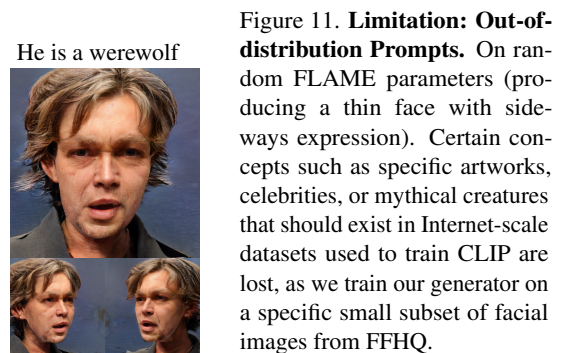


Figure 11. **Limitation: Out-of-distribution Prompts.** On random FLAME parameters (producing a thin face with sideways expression). Certain concepts such as specific artworks, celebrities, or mythical creatures that should exist in Internet-scale datasets used to train CLIP are lost, as we train our generator on a specific small subset of facial images from FFHQ.

and do not consider 3D-aware face generation. For text-to-3D face generation, existing methods [1, 56] build on 3D morphable face models and generate 3D faces with geometry and texture. Owing to the parametric model, these approaches can explicitly control expression, pose; however, the generation results lack shape variation. To address shape variation, TG-3DFace [52] proposed text-to-face cross-modal alignment for high-quality 3D-aware face synthesis. This method has two limitations: 1) lack of explicit 3D geometry control, and 2) requirement of text annotated training dataset. Table 3 compares existing text-to-3D face generation methods. Ours is the only method that allows text-guided synthesis of high-quality 3D portraits with explicit geometry/camera control from an unlabelled 2D dataset.

## 6. Limitations and Conclusion

**Limitations.** While we enable generation using prompts via an LVLm, there are bounds. As we train a generator on a specific dataset like FFHQ and we disentangle CLIP with respect to that dataset, prompting for attributes that are not represented in the data samples or identity information will not work well (Fig. 11). A generative approach will struggle to represent a diverse set of people if the data is not diverse, e.g., FFHQ has known skin tone biases; practical deployment must carefully avoid such biases.

**Conclusion.** Our main contribution is to identify a fundamental problem with LVLms—more specifically with their alignment objectives—that makes them difficult to use as plug-in text-conditioners within 3D generators. Demonstrated on top of an EG3D backbone architecture, we pro-

pose regularization and canonicalisation techniques that (i) effectively disentangle 3D factors from CLIP, and (ii) avoids distribution collapse that otherwise leads to low diversity and low quality output. We demonstrate that our techniques can be important to language-guided portrait synthesis through experiments against current approaches.

## References

- [1] Shivangi Aneja, Justus Thies, Angela Dai, and Matthias Nießner. Clipface: Text-guided editing of textured 3d morphable models. In *ACM SIGGRAPH 2023 Conference Proceedings*, pages 1–11, 2023. 7, 8, 13
- [2] Alexander W. Bergman, Petr Kellnhofer, Yifan Wang, Eric R. Chan, David B. Lindell, and Gordon Wetzstein. Generative neural articulated radiance fields. In *NeurIPS*, 2022. 1, 2, 3, 4, 7, 8, 12
- [3] Mikołaj Bińkowski, Danica J Sutherland, Michael Arbel, and Arthur Gretton. Demystifying mmd gans. *arXiv preprint arXiv:1801.01401*, 2018. 7
- [4] Zehranaz Canfes, M Furkan Atasoy, Alara Dirik, and Pinar Yanardag. Text and image guided 3d avatar generation and manipulation. In *Proceedings of the IEEE/CVF Winter Conference on Applications of Computer Vision*, pages 4421–4431, 2023. 7
- [5] Eric R. Chan, Connor Z. Lin, Matthew A. Chan, Koki Nagano, Boxiao Pan, Shalini De Mello, Orazio Gallo, Leonidas Guibas, Jonathan Tremblay, Sameh Khamis, Tero Karras, and Gordon Wetzstein. Efficient geometry-aware 3D generative adversarial networks. In *CVPR*, 2022. 3, 4, 7, 8
- [6] Yiji Cheng, Fei Yin, Xiaoke Huang, Xintong Yu, Jiayang Liu, Shikun Feng, Yujia Yang, and Yansong Tang. Efficient text-guided 3d-aware portrait generation with score distillation sampling on distribution. *arXiv preprint arXiv:2306.02083*, 2023. 7, 12, 13
- [7] Xuangeng Chu and Tatsuya Harada. Generalizable and animatable gaussian head avatar. *arXiv preprint arXiv:2410.07971*, 2024. 2
- [8] Antonia Creswell, Tom White, Vincent Dumoulin, Kai Arulkumaran, Biswa Sengupta, and Anil A Bharath. Generative adversarial networks: An overview. *IEEE signal processing magazine*, 35(1):53–65, 2018. 7
- [9] Ming Ding, Zhuoyi Yang, Wenyi Hong, Wendi Zheng, Chang Zhou, Da Yin, Junyang Lin, Xu Zou, Zhou Shao, Hongxia Yang, et al. Cogview: Mastering text-to-image generation via transformers. *Advances in Neural Information Processing Systems*, 34:19822–19835, 2021. 8
- [10] Ming Ding, Wendi Zheng, Wenyi Hong, and Jie Tang. Cogview2: Faster and better text-to-image generation via hierarchical transformers. *Advances in Neural Information Processing Systems*, 35:16890–16902, 2022. 8
- [11] Hao Dong, Simiao Yu, Chao Wu, and Yike Guo. Semantic image synthesis via adversarial learning. In *Proceedings of the IEEE international conference on computer vision*, pages 5706–5714, 2017. 8
- [12] Patrick Esser, Robin Rombach, Andreas Blattmann, and Bjorn Ommer. Imagebart: Bidirectional context with multinomial diffusion for autoregressive image synthesis. *Advances in neural information processing systems*, 34:3518–3532, 2021. 8
- [13] Yao Feng, Haiwen Feng, Michael J. Black, and Timo Bolkart. Learning an animatable detailed 3D face model from in-the-wild images. 2021. 3
- [14] Ian Goodfellow, Jean Pouget-Abadie, Mehdi Mirza, Bing Xu, David Warde-Farley, Sherjil Ozair, Aaron Courville, and Yoshua Bengio. Generative adversarial nets. *Advances in neural information processing systems*, 27, 2014. 13
- [15] Martin Heusel, Hubert Ramsauer, Thomas Unterthiner, Bernhard Nessler, and Sepp Hochreiter. Gans trained by a two time-scale update rule converge to a local nash equilibrium. *Advances in neural information processing systems*, 30, 2017. 7
- [16] Jonathan Ho, Ajay Jain, and Pieter Abbeel. Denoising diffusion probabilistic models. *Advances in neural information processing systems*, 33:6840–6851, 2020. 8
- [17] Yiwen Huang, Zhiqiu Yu, Xinjie Yi, Yue Wang, and James Tompkin. Removing the quality tax in controllable face generation. In *Proceedings of the IEEE/CVF Winter Conference on Applications of Computer Vision (WACV)*, pages 5364–5373, 2024. 4
- [18] Sangeek Hyun and Jae-Pil Heo. Adversarial generation of hierarchical gaussians for 3d generative model. *arXiv preprint arXiv:2406.02968*, 2024. 2
- [19] Nikolay Jetchev. Clipmatrix: Text-controlled creation of 3d textured meshes. *arXiv preprint arXiv:2109.12922*, 2021. 7
- [20] Tero Karras, Samuli Laine, and Timo Aila. A style-based generator architecture for generative adversarial networks. In *Proceedings of the IEEE/CVF Conference on Computer Vision and Pattern Recognition*, pages 4401–4410, 2019. 2, 6, 7
- [21] Tero Karras, Samuli Laine, Miika Aittala, Janne Hellsten, Jaakko Lehtinen, and Timo Aila. Analyzing and improving the image quality of stylegan. In *Proceedings of the IEEE/CVF conference on computer vision and pattern recognition*, pages 8110–8119, 2020. 7
- [22] Tobias Kirschstein, Simon Giebenhain, Jiapeng Tang, Markos Georgopoulos, and Matthias Nießner. Gghead: Fast and generalizable 3d gaussian heads. *arXiv preprint arXiv:2406.09377*, 2024. 2
- [23] Yushi Lan, Feitong Tan, Di Qiu, Qiangeng Xu, Kyle Genova, Zeng Huang, Sean Fanello, Rohit Pandey, Thomas Funkhouser, Chen Change Loy, and Yinda Zhang. Gaussian3diff: 3d gaussian diffusion for 3d full head synthesis and editing. In *ECCV*, 2024. 2
- [24] Doyup Lee, Chiheon Kim, Saehoon Kim, Minsu Cho, and Wook-Shin Han. Autoregressive image generation using residual quantization. In *Proceedings of the IEEE/CVF Conference on Computer Vision and Pattern Recognition*, pages 11523–11532, 2022. 8
- [25] Bowen Li, Xiaojuan Qi, Thomas Lukasiewicz, and Philip Torr. Controllable text-to-image generation. *Advances in Neural Information Processing Systems*, 32, 2019. 7, 8
- [26] Tianye Li, Timo Bolkart, Michael. J. Black, Hao Li, and Javier Romero. Learning a model of facial shape and expres-

- sion from 4D scans. *ACM Transactions on Graphics, (Proc. SIGGRAPH Asia)*, 36(6):194:1–194:17, 2017. 1, 3, 7
- [27] Victor Weixin Liang, Yuhui Zhang, Yongchan Kwon, Serena Yeung, and James Y Zou. Mind the gap: Understanding the modality gap in multi-modal contrastive representation learning. *Advances in Neural Information Processing Systems*, 35:17612–17625, 2022. 2
- [28] Haotian Liu, Chunyuan Li, Qingyang Wu, and Yong Jae Lee. Visual instruction tuning. *Advances in neural information processing systems*, 36, 2024. 2
- [29] Lars Mescheder, Andreas Geiger, and Sebastian Nowozin. Which training methods for gans do actually converge? In *International conference on machine learning*, pages 3481–3490. PMLR, 2018. 13
- [30] Oscar Michel, Roi Bar-On, Richard Liu, Sagie Benaim, and Rana Hanocka. Text2mesh: Text-driven neural stylization for meshes. In *Proceedings of the IEEE/CVF Conference on Computer Vision and Pattern Recognition*, pages 13492–13502, 2022. 7
- [31] Osaid Rehman Nasir, Shailesh Kumar Jha, Manraj Singh Grover, Yi Yu, Ajit Kumar, and Rajiv Ratn Shah. Text2facegan: Face generation from fine grained textual descriptions. In *2019 IEEE Fifth International Conference on Multimedia Big Data (BigMM)*, pages 58–67. IEEE, 2019. 8
- [32] Alex Nichol, Prafulla Dhariwal, Aditya Ramesh, Pranav Shyam, Pamela Mishkin, Bob McGrew, Ilya Sutskever, and Mark Chen. Glide: Towards photorealistic image generation and editing with text-guided diffusion models. *arXiv preprint arXiv:2112.10741*, 2021. 8
- [33] Aaron van den Oord, Yazhe Li, and Oriol Vinyals. Representation learning with contrastive predictive coding. *arXiv preprint arXiv:1807.03748*, 2018. 2
- [34] P. Paysan, R. Knothe, B. Amberg, S. Romdhani, and T. Vetter. A 3d face model for pose and illumination invariant face recognition. Genova, Italy, 2009. IEEE. 1
- [35] Jun Peng, Han Pan, Yiyi Zhou, Jing He, Xiaoshuai Sun, Yan Wang, Yongjian Wu, and Rongrong Ji. Towards open-ended text-to-face generation, combination and manipulation. In *Proceedings of the 30th ACM International Conference on Multimedia*, pages 5045–5054, 2022. 8
- [36] Alec Radford, Jong Wook Kim, Chris Hallacy, Aditya Ramesh, Gabriel Goh, Sandhini Agarwal, Girish Sastry, Amanda Askell, Pamela Mishkin, Jack Clark, et al. Learning transferable visual models from natural language supervision. In *International conference on machine learning*, pages 8748–8763. PMLR, 2021. 1, 2
- [37] Aditya Ramesh, Mikhail Pavlov, Gabriel Goh, Scott Gray, Chelsea Voss, Alec Radford, Mark Chen, and Ilya Sutskever. Zero-shot text-to-image generation. In *International Conference on Machine Learning*, pages 8821–8831. PMLR, 2021. 8
- [38] Aditya Ramesh, Prafulla Dhariwal, Alex Nichol, Casey Chu, and Mark Chen. Hierarchical text-conditional image generation with clip latents. *arXiv preprint arXiv:2204.06125*, 1(2): 3, 2022. 8
- [39] Scott Reed, Zeynep Akata, Xinchen Yan, Lajanugen Logeswaran, Bernt Schiele, and Honglak Lee. Generative adversarial text to image synthesis. In *International conference on machine learning*, pages 1060–1069. PMLR, 2016. 8
- [40] Salah Rifai, Grégoire Mesnil, Pascal Vincent, Xavier Muller, Yoshua Bengio, Yann Dauphin, and Xavier Glorot. Higher order contractive auto-encoder. In *Machine Learning and Knowledge Discovery in Databases*, pages 645–660, Berlin, Heidelberg, 2011. Springer Berlin Heidelberg. 12
- [41] Robin Rombach, Andreas Blattmann, Dominik Lorenz, Patrick Esser, and Björn Ommer. High-resolution image synthesis with latent diffusion models. 2022 ieee. In *CVF Conference on Computer Vision and Pattern Recognition (CVPR)*, pages 10674–10685, 2021. 8
- [42] Chitwan Saharia, William Chan, Saurabh Saxena, Lala Li, Jay Whang, Emily L Denton, Kamyar Ghasemipour, Raphael Gontijo Lopes, Burcu Karagol Ayan, Tim Salimans, et al. Photorealistic text-to-image diffusion models with deep language understanding. *Advances in Neural Information Processing Systems*, 35:36479–36494, 2022. 8
- [43] David Stap, Maurits Bleeker, Sarah Ibrahimi, and Maartje Ter Hoeve. Conditional image generation and manipulation for user-specified content. *arXiv preprint arXiv:2005.04909*, 2020. 8
- [44] Jianxin Sun, Qi Li, Weining Wang, Jian Zhao, and Zhenan Sun. Multi-caption text-to-face synthesis: Dataset and algorithm. In *Proceedings of the 29th ACM International Conference on Multimedia*, pages 2290–2298, 2021. 7, 8
- [45] Ming Tao, Hao Tang, Songsong Wu, Nicu Sebe, Fei Wu, Xiao-Yuan Jing, et al. Df-gan: Deep fusion generative adversarial networks for text-to-image synthesis. *arXiv preprint arXiv:2008.05865*, 2(6), 2020. 8
- [46] Ashish Vaswani, Noam Shazeer, Niki Parmar, Jakob Uszkoreit, Llion Jones, Aidan N Gomez, Łukasz Kaiser, and Illia Polosukhin. Attention is all you need. *Advances in neural information processing systems*, 30, 2017. 8
- [47] Tianren Wang, Teng Zhang, and Brian Lovell. Faces a la carte: Text-to-face generation via attribute disentanglement. In *Proceedings of the IEEE/CVF winter conference on applications of computer vision*, pages 3380–3388, 2021. 8
- [48] Menghua Wu, Hao Zhu, Linjia Huang, Yiyu Zhuang, Yuanxun Lu, and Xun Cao. High-fidelity 3d face generation from natural language descriptions. In *Proceedings of the IEEE/CVF Conference on Computer Vision and Pattern Recognition*, pages 4521–4530, 2023. 7
- [49] Weihao Xia, Yujiu Yang, Jing-Hao Xue, and Baoyuan Wu. Tedigan: Text-guided diverse face image generation and manipulation. In *Proceedings of the IEEE/CVF conference on computer vision and pattern recognition*, pages 2256–2265, 2021. 6, 7, 8
- [50] Hongyi Xu, Guoxian Song, Zihang Jiang, Jianfeng Zhang, Yichun Shi, Jing Liu, Wanchun Ma, Jiashi Feng, and Linjie Luo. Omniaavatar: Geometry-guided controllable 3d head synthesis. In *Proceedings of the IEEE/CVF Conference on Computer Vision and Pattern Recognition*, pages 12814–12824, 2023. 8
- [51] Tao Xu, Pengchuan Zhang, Qiuyuan Huang, Han Zhang, Zhe Gan, Xiaolei Huang, and Xiaodong He. AttnGAN: Fine-grained text to image generation with attentional generative

- adversarial networks. In *Proceedings of the IEEE conference on computer vision and pattern recognition*, pages 1316–1324, 2018. [7](#), [8](#)
- [52] Cuican Yu, Guansong Lu, Yihan Zeng, Jian Sun, Xiaodan Liang, Huibin Li, Zongben Xu, Songcen Xu, Wei Zhang, and Hang Xu. Towards high-fidelity text-guided 3d face generation and manipulation using only images. In *Proceedings of the IEEE/CVF International Conference on Computer Vision*, pages 15326–15337, 2023. [7](#), [8](#), [13](#)
- [53] Jiahui Yu, Yuanzhong Xu, Jing Yu Koh, Thang Luong, Gunjan Baid, Zirui Wang, Vijay Vasudevan, Alexander Ku, Yinfei Yang, Burcu Karagol Ayan, et al. Scaling autoregressive models for content-rich text-to-image generation. *arXiv preprint arXiv:2206.10789*, 2(3):5, 2022. [8](#)
- [54] Han Zhang, Tao Xu, Hongsheng Li, Shaoting Zhang, Xiaogang Wang, Xiaolei Huang, and Dimitris N Metaxas. Stackgan: Text to photo-realistic image synthesis with stacked generative adversarial networks. In *Proceedings of the IEEE international conference on computer vision*, pages 5907–5915, 2017. [8](#)
- [55] Han Zhang, Tao Xu, Hongsheng Li, Shaoting Zhang, Xiaogang Wang, Xiaolei Huang, and Dimitris N Metaxas. Stackgan++: Realistic image synthesis with stacked generative adversarial networks. *IEEE transactions on pattern analysis and machine intelligence*, 41(8):1947–1962, 2018. [8](#)
- [56] Longwen Zhang, Qiwei Qiu, Hongyang Lin, Qixuan Zhang, Cheng Shi, Wei Yang, Ye Shi, Sibe Yang, Lan Xu, and Jingyi Yu. Dreamface: Progressive generation of animatable 3d faces under text guidance. *arXiv preprint arXiv:2304.03117*, 2023. [8](#)
- [57] Zhu Zhang, Jianxin Ma, Chang Zhou, Rui Men, Zhikang Li, Ming Ding, Jie Tang, Jingren Zhou, and Hongxia Yang. M6-ufc: Unifying multi-modal controls for conditional image synthesis via non-autoregressive generative transformers. *arXiv preprint arXiv:2105.14211*, 2021. [8](#)
- [58] Junsheng Zhou, Weiqi Zhang, and Yu-Shen Liu. Diffggs: Functional gaussian splatting diffusion. *arXiv preprint arXiv:2410.19657*, 2024. [2](#)
- [59] Yutong Zhou. Generative adversarial network for text-to-face synthesis and manipulation. In *Proceedings of the 29th ACM International Conference on Multimedia*, pages 2940–2944, 2021. [1](#)
- [60] Yutong Zhou and Nobutaka Shimada. Generative adversarial network for text-to-face synthesis and manipulation with pretrained bert model. In *2021 16th IEEE International Conference on Automatic Face and Gesture Recognition (FG 2021)*, pages 01–08, 2021. [7](#)
- [61] Minfeng Zhu, Pingbo Pan, Wei Chen, and Yi Yang. Dm-gan: Dynamic memory generative adversarial networks for text-to-image synthesis. In *Proceedings of the IEEE/CVF conference on computer vision and pattern recognition*, pages 5802–5810, 2019. [8](#)

## Appendices

### A. Proof of the stochastic approximator of the Jacobian

Given a vector function  $f : \mathbb{R}^M \rightarrow \mathbb{R}^N$  and its variable  $x \in \mathbb{R}^M$ , the Jacobian  $\mathbf{J} \in \mathbb{R}^{N \times M}$  of  $f$ , we propose the following two stochastic approximators for  $\|\mathbf{J}\|_F^2$ :

$$\|\mathbf{J}\|_F^2 = \mathbb{E}_{v \sim \mathcal{N}(0, I_M)} \left[ \|\mathbf{J}v\|^2 \right] \quad (22)$$

$$\|\mathbf{J}\|_F^2 = \lim_{\sigma \rightarrow 0} \mathbb{E}_{\epsilon \sim \mathcal{N}(0, \sigma^2 I_M)} \left[ \frac{1}{\sigma^2} \|f(x + \epsilon) - f(x)\|^2 \right] \quad (23)$$

Our proofs follow the same principles as the numerical approximation of the Hessian matrix norm in [40]. While evaluating  $\|\mathbf{J}\|_F^2$  naively using `torch.autograd.functional.jacobian` is impractically slow, Equation (22) can be efficiently evaluated by `torch.autograd.functional.jvp`. Equation (23) is an even faster finite difference approximation that we use in the main paper for  $R_{\mathbf{r}_x}$ .

**Proof for Equation (22).** Note that for  $i \neq j$ ,  $\mathbb{E}[v_i v_j] = \mathbb{E}[v_i] \mathbb{E}[v_j] = 0$ . For  $i = j$ ,  $\mathbb{E}[v_i v_j] = \mathbb{E}[v_i^2] = 1$ .

$$\mathbb{E}_{v \sim \mathcal{N}(0, I_M)} \left[ \|\mathbf{J}v\|^2 \right] \quad (24)$$

$$= \mathbb{E} \left[ \left\langle \sum_{i=1}^M v_i \frac{\partial f}{\partial x_i}, \sum_{i=1}^M v_i \frac{\partial f}{\partial x_i} \right\rangle \right] \quad (25)$$

$$= \sum_{i=1}^M \sum_{j=1}^M \mathbb{E}[v_i v_j] \left\langle \frac{\partial f}{\partial x_i}, \frac{\partial f}{\partial x_j} \right\rangle \quad (26)$$

$$= \sum_{i=1}^M \left\langle \frac{\partial f}{\partial x_i}, \frac{\partial f}{\partial x_i} \right\rangle \quad (27)$$

$$= \|\mathbf{J}\|_F^2 \quad (28)$$

**Proof for Equation (23).** Apply Taylor expansion to  $f(x + \epsilon)$  at  $x$ :

$$f(x + \epsilon) = f(x) + \mathbf{J}\epsilon + R(x, \epsilon) \quad (29)$$

where

$$R(x, \epsilon) = \sum_{K=2}^{\infty} \frac{1}{K!} \sum_{i_1, \dots, i_K} \epsilon_{i_1} \dots \epsilon_{i_K} \frac{\partial^K f}{\partial x_{i_1} \dots \partial x_{i_K}} \quad (30)$$

which gives us

$$\lim_{\sigma \rightarrow 0} \mathbb{E}_{\epsilon \sim \mathcal{N}(0, \sigma^2 I_M)} \left[ \frac{1}{\sigma^2} \|f(x + \epsilon) - f(x)\|^2 \right] \quad (31)$$

$$= \lim_{\sigma \rightarrow 0} \mathbb{E} \left[ \frac{1}{\sigma^2} \|\mathbf{J}\epsilon + R(x, \epsilon)\|^2 \right] \quad (32)$$

$$= \lim_{\sigma \rightarrow 0} \mathbb{E} \left[ \frac{1}{\sigma^2} \|\mathbf{J}\epsilon\|^2 \right] + \lim_{\sigma \rightarrow 0} \mathbb{E} \left[ \frac{2}{\sigma^2} \langle \mathbf{J}\epsilon, R(x, \epsilon) \rangle \right] + \lim_{\sigma \rightarrow 0} \mathbb{E} \left[ \frac{1}{\sigma^2} \langle R(x, \epsilon), R(x, \epsilon) \rangle \right] \quad (33)$$

$$= \|\mathbf{J}\|_F^2 + \lim_{\sigma \rightarrow 0} \mathbb{E} \left[ \frac{2}{\sigma^2} \langle \mathbf{J}\epsilon, R(x, \epsilon) \rangle \right] + \lim_{\sigma \rightarrow 0} \mathbb{E} \left[ \frac{1}{\sigma^2} \langle R(x, \epsilon), R(x, \epsilon) \rangle \right]. \quad (34)$$

We now analyze  $\epsilon_{i_1} \dots \epsilon_{i_K}$ , which can be rewritten to  $\epsilon_1^{p_1} \dots \epsilon_M^{p_M}$  where  $p_1 + \dots + p_M = K$ . Note that  $\langle \mathbf{J}\epsilon, R(x, \epsilon) \rangle$  and  $\langle R(x, \epsilon), R(x, \epsilon) \rangle$  imply  $K \geq 3$  as we have  $K \geq 2$  from  $R(x, \epsilon)$ . In such scenario,

- Either there is at least one odd element in  $\{p_1, \dots, p_M\}$  and  $\mathbb{E}[\epsilon_{i_1} \dots \epsilon_{i_K}] = 0$  because odd moments of a zero mean Gaussian are zero,
- Or  $p_1, \dots, p_M$  are all even but  $\mathbb{E}[\epsilon_{i_1} \dots \epsilon_{i_K}]$  is a higher order infinitesimal than  $\sigma^2$ , and we have  $\lim_{\sigma \rightarrow 0} \frac{1}{\sigma^2} \mathbb{E}[\epsilon_{i_1} \dots \epsilon_{i_K}] = 0$ .

Therefore:

$$\lim_{\sigma \rightarrow 0} \mathbb{E} \left[ \frac{2}{\sigma^2} \langle \mathbf{J}\epsilon, R(x, \epsilon) \rangle \right] \quad (35)$$

$$= \lim_{\sigma \rightarrow 0} \mathbb{E} \left[ \frac{1}{\sigma^2} \langle R(x, \epsilon), R(x, \epsilon) \rangle \right] = 0. \quad \blacksquare \quad (36)$$

To implement  $R_{\mathbf{r}_x}$ , we empirically set  $\sigma = 0.1$ . We experimented with using 1, 2, 4 and 8  $\epsilon$  vectors for the expectation, but found no significant difference and thus settled for using only one  $\epsilon$  vector to minimize the computation cost.

### B. Implementation Details

Our implementation extends the official PyTorch implementation<sup>2</sup> of EG3D [6]. We initialize the generator backbone with the weights from the official checkpoint provided by the authors. For the most part, we follow the training strategies of EG3D. However, we drop the second training stage of EG3D and fix neural rendering resolution to  $64 \times 64$  due to computation budget limitations. We opt for lower initial learning rates  $\gamma = 0.001$  for both generator  $G$  and discriminator  $D$  rather than 0.0025 for  $G$  and 0.002 for  $D$ . We also remove the generator pose conditioning, as mentioned in the main paper.

For deformation, we use the surface-field implementation from GNARF by Bergman et al. [2]. For faster deformation

<sup>2</sup><https://github.com/NVlabs/eg3d>

computation, we simplify the FLAME mesh to 2500 triangles. However, we use the full mesh for generating the mesh render  $rdr$  in discriminator conditioning.

For objectives, we follow EG3D and use a non-saturating adversarial loss [14],  $R_1$  gradient penalty [29], and density regularization [6]. We additionally append our regularizations  $R_{r_{\hat{x}}}$  and  $R_{\text{norm}}$  to the training objectives, and empirically set their weights to 0.01 and 10 respectively.

### C. Text-Guided Appearance Editing.

In addition to text conditional generation, our model is also capable of fine-grained editing of existing portraits. The nature of editing is no different from alignment: we can adopt a specialized alignment network  $E_t$  to align any style vector  $w$  to our editing request  $t$  similarly to Equation (11) in the main paper:

$$w_t(\alpha) = w + \alpha E_t(w) \quad (37)$$

$t$  is represented by text prompts such as “blonde”, “blue eyes”, etc., and  $\alpha$  controls the editing strength. We hypothesize that the  $\mathcal{W}^+$  space is sufficiently disentangled for local editing, i.e., it is achievable to apply the desired effect while preserving the rest of the portrait by manipulating  $w$ . A similar design has been proposed by Aneja et al. [1] in the context of textured 3DMM editing.

The training scheme of  $E_t$  remains a question. While it is possible to optimize  $E_t$  using an adversarial objective as with  $T_G$ , the problem with the adversarial loss is that it encourages alignment but not disentanglement. There is no incentive to preserve the content of the initial portrait while applying the desired effect, thus making it unsuitable for editing. To promote disentanglement, we adopt the contrastive CLIP loss from Aneja et al. [1] that allows us to single out the components related to  $t$  and modify them. We render the initial portrait and the edited portrait under a neutral camera pose and 3DMM parameters. Then, the change induced by  $E_t$  in the CLIP embedding space is given by:

$$\Delta x = E_{\text{img}}(G(w_t, \mathbf{c}_{\text{n.cam}}, \mathbf{c}_{\text{n.geo}})) - E_{\text{img}}(G(w, \mathbf{c}_{\text{n.cam}}, \mathbf{c}_{\text{n.geo}})) \quad (38)$$

Meanwhile, we define a template prompt  $\bar{t}$  = “a photo of a neutral face” and the expected change induced by  $t$  is:

$$\Delta t = E_{\text{txt}}(t) - E_{\text{txt}}(\bar{t}) \quad (39)$$

We freeze  $G$  and train  $E_t$  with the objective of aligning  $\Delta x$  to  $\Delta t$ . We additionally apply  $R_{\text{norm}}$ : without norm growth regularization, we observe instant collapse early in the training. The full training objective is:

$$1 - \frac{\Delta x \Delta t}{\|\Delta x\| \|\Delta t\|} + \eta R_{\text{norm}} \quad (40)$$

where  $\eta$  is empirically set to 10. We visualize our editing results in Figure 12. Although a similar training objective is adopted at inference time in TG-3DFace [52], our editing results are considerably more realistic and disentangled as we do not update  $G$  (main paper Figure 9).

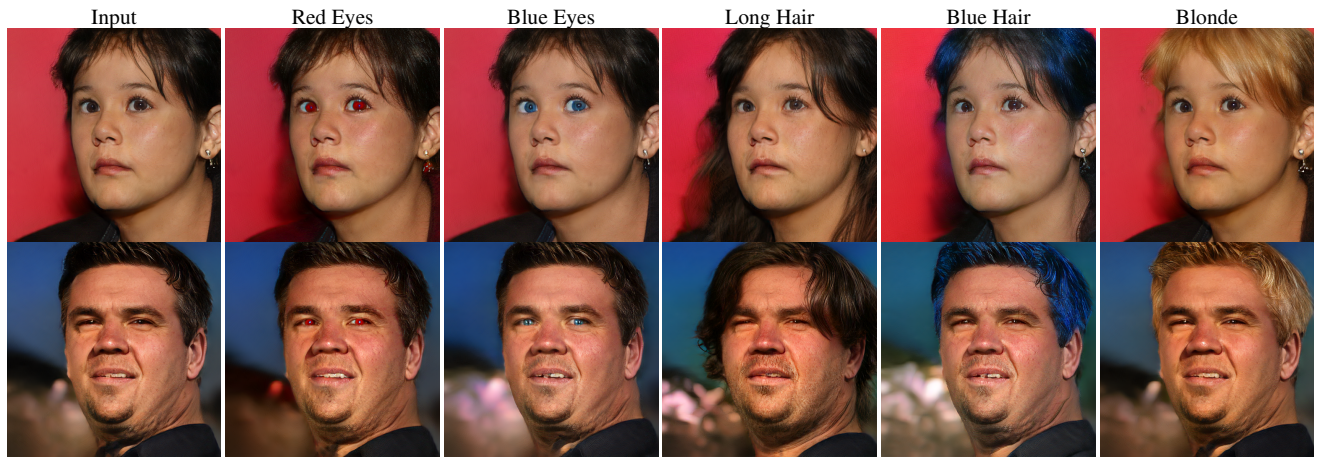


Figure 12. Text-guided appearance editing results.